Structural Engineering and Mechanics, *Vol. 73, No. 6 (2020) 685-698*
DOI: https://doi.org/10.12989/sem.2020.73.6.685

Size-dependent dynamic stability of a FG polymer microbeam reinforced by graphene oxides

Yuewu Wang[1a], Ke Xie[2b] and Tairan Fu*[1]

[1]Key Laboratory for Thermal Science and Power Engineering of Ministry of Education, Beijing Key Laboratory of CO2 Utilization and Reduction Technology, Department of Energy and Power Engineering, Tsinghua University, Beijing, China, 100084
[2]Institute of Systems Engineering, China Academy of Engineering Physics, Mianyang, Sichuan, China, 621900

(Received July 4, 2019, Revised October 16, 2019, Accepted November 12, 2019)

Abstract. The dynamic stability of a functionally graded polymer microbeam reinforced by graphene oxides subjected to a periodic axial force is investigated. The microbeam is assumed to rest on an elastic substrate and is subjected to various immovable boundary restraints. The weight fraction of graphene oxides nanofillers is graded across the beam thickness. The effective Young's modulus of the functionally graded graphene oxides reinforced composite (FG-GORC) was determined using modified Halpin–Tsai model, with the mixture rule used to evaluate the effective Poisson's ratio and the mass density. An improved third order shear deformation theory (TSDT) is used in conjunction with the Chebyshev polynomial-based Ritz method to derive the Mathieu-Hill equations for dynamic stability of the FG-GORC microbeam, in which the scale effect is taken into account based on modified couple stress theory. Then, the Mathieu-Hill equation was solved using Bolotin's method to predict the principle unstable regions of the FG-GORC microbeams. The numerical results show the effects of the small scale, the graphene oxides nanofillers as well as the elastic substrate on the dynamic stability behaviors of the FG-GORC microbeams.

Keywords: functionally graded microbeam; graphene oxide reinforced composites; dynamic stabilities; third order shear deformation theory; Chebyshev-Ritz method

1. Introduction

Polymers can be easily machined so they are useful materials for fabricating microactuators with lower energy consumption and microsensors with higher detection sensitivities. However, actuators and sensors made of pure polymers are often restricted to low speeds, small forces, slow frequency responses and short dynamic ranges to name only a few limitations (Li *et al*. 2003, Li *et al.* 2008, Ashrafi *et al.* 2006, Ramaratnam *et al.* 2006, Rokni *et al.* 2012a, Rokni *et al.* 2012b). Therefore, many scientists have sought to develop high-strength, multifunctional polymer-based nanocomposites by adding nanofillers into the polymer matrix as reinforcements to improve their mechanical, thermal and electrical properties and make them applicable in a wider range of applications.

Functionally graded material (FGM) is a novel composite that has been widely used in many engineering fields. Nano-/micro-structural components made of FGMs excited great interests of researchers and engineers (Ebrahimi and Barati 2016a, Ebrahimi and Barati 2016b, Ebrahimi and Salari 2015a, Ebrahimi *et al.* 2015b). Some nonlocal models have been proposed and implemented to deal with mechanical responses of FG nano-structures based on the mid-plane (Ebrahimi and Barati 2017a, Ebrahimi and Barati 2017b, Ebrahimi and Dabbagh 2017) and physical neutral surface (Ebrahimi and Salari 2015c). The smoothly graded material properties offers a smooth stress distribution with structures so that the remarkable stress mismatch that leads to interfacial failure in the conventional laminates can be avoided. Thus, FGM is a suitable composite applied in thermal enviroments. It is worth to mention that Ebrahimi and his co-authors devoted great efforts of addressing the thermal effects on mechanical behaviors of FG nano-materials and published a series of works (Ebrahimi and Salari 2016, Ebrahimi and Barati 2017c, Ebrahimi *et al*. 2017d, Ebrahimi and Hosseini 2016, Ebrahimi and Barati 2018a, Ebrahimi *et al*. 2016). In addition, the effects of porosities within the FG-nanomaterials on the nano-structures are also considered (Ebrahimi and Mokhtari 2015, Ebrahimi and Barati 2017d).In recent, the combination of functionally graded material (FGM) and polymer-based nanomaterials introduces the functionally graded polymer-based nanocomposites, in which the contents of nanofillers are dispersed within polymer matrix uniformly or no-uniformly. These kinds of nanocomposites are taken as ideal raw materials to fabricate microsensors and microactuators, because they preserve the flexibility of tailoring coming of polymer and obtained improved performances from nano-reinforcements.

Graphene nanoplatelets (GNPs) are excellent candidates for fabricating polymer-based nanocomposites, such nanocomposites have been used extensively (Yang *et al.* 2010, Potts *et al.* 2011). GNP-reinforced composites (Wang

*Corresponding author, Professor
E-mail: trfu@tsinghua.edu.cn; wang_yuewu@qq.com
[a] Ph.D.
[b] Ph.D.

http://www.techno-press.com/journals/sem&subpage=7
ISSN: 1225-4568 (Print), 1598-6217 (Online)

et al. 2016, Song *et al.* 2016, Wang *et al.* 2019a, Mao *et al.* 2019, Arefi *et al.* 2018, Javani *et al.* 2019) have also been introduced, in which the weight fractions of the GNPs vary in the thickness direction, to better utilize the superior mechanical properties of the carbon-based nanofiller. The mechanical response of the macro/nano structures in GNP-reinforced composites have been investigated extensively (Karami *et al.* 2019, Wang *et al.* 2019b). However, as graphene is expensive and relatively hard to produce, many efforts have been made to find effective yet inexpensive ways to make and use graphene derivatives or related materials such as graphene oxide. Graphene oxide (GO) is a single-atomic layer material made by oxidation of graphite which is cheap and abundant (Graphene-info 2019). Graphene oxide is an oxidized form of graphene which is laced with oxygen-containing groups with a large surface area. Graphene oxide can be easily mixed with various polymers to enhance the properties of the composite materials like the tensile strength, elasticity, conductivity and others (Mahka *et al.* 2015). Therefore, the mechanical properties of a functionally graded polymer composite structure reinforced by graphene oxide should be investigated.

This study investigated the dynamic stability of a functionally graded graphene oxide reinforced nanocomposite (FG-GORC) microbeam because beam-like structures are the most common structural components in nano/micro and macro scale engineered systems (Wattanasakulpong *et al.* 2018, Arani *et al.* 2018, Setoodeh and Rezae 2017), and these structural components may become instable with compressive periodic loads even if the load is below the critical buckling load. Thus, the dynamic stability of micro scale composite beams experiencing periodic loads needs further study. Ke *et al.* (2013) investigated the dynamic stability of functionally graded carbon nanotube reinforced composite beams and FGM microbeams using Timoshenko beam theory. Ebrahimi and Barati (2018b) performed a stability analysis of porous multi-phase nanocrystalline nonlocal beams. Mohammed and Cagri (2018) investigated the dynamic stability of functionally graded (FG) size-dependent sandwich microbeams subjected to parametric axial excitations based on nonlocal strain gradient theory. Wu *et al.* (2017) studied the dynamic stability of functionally graded multilayer nanocomposite beams reinforced with a low percentage of GNPs subjected to the combined action of a periodic axial force and a temperature change. Chen et al. (2019) analyzed the size dependent free vibration, buckling and dynamic stability of bi-directional functionally graded microbeams embedded in an elastic medium using a third order shear deformation theory. Saemul and Ganesan (2018) investigated the dynamic stability of doubly tapered cantilever composite beams rotating with a periodic rotational velocity. This literature review suggests that the dynamic stability of composite beams has been widely investigated, but few studies have focused on the dynamic stability of microbeams made of functionally graded polymer nanocomposites reinforced by GOs. Evaluating dynamic stability behaviors of FG-GORC microbeams has potential application values for developing polymer-based microactuators and micro robots, which is always a hot point and front line gambit in bioengineering, micro-nanofabrications, and intelligent structures.

To the authors' knowledge, the present work is the first investigation of dynamic stability of a functionally graded polymer microbeam reinforced by graphene oxides subjected to a periodic axial force while resting on an elastic substrate. A FG-GORC microbeam is proposed based on the modified Halpin–Tsai model and the mixture rule in the first section of following part. The effective material properties, such as the Young's modulus, mass density and Poisson's ratio, are determined. Then, in order to deal with small-scale effects within microstructures, a modified couple stress-based beam theory is developed by using an improved third order shear deformation theory (TSDT) with inclusions of couple stress tensors. The Mathieu-Hill equations for the dynamic stability of FG-GORC microbeams with various boundary conditions are derived using Chebyshev polynomial-based Ritz method and solved via Bolotin's method to find principle unstable regions of FG-GORC microbeams resting on the elastic substrate. At last section, some parameter studies are performed to show the effects of the small scale, graphene oxide nanofillers, elastic substrate and boundary conditions on the dynamic stability of the FG-GORC microbeams. The present work provides an effective evaluation model for stability behaviors of FG-GORC microbeams, and the results are helpful to addressing reinforced effects of GO nanofillers on polymer-based microstructures.

2. FG-GORC microbeam

Fig. 1 shows a schematic of a FG-GORC microbeam resting on an elastic substrate and subjected to a periodic axial force $P(t)$, where t is time. The length, width, and thickness of the beam are L, b, and h, respectively, and the coordinate system origin is fixed at the center of the left end of the beam. The beam is assumed to rest on a Winkler–Pasternak type elastic substrate with a Winkler stiffness of k_W and a Pasternak stiffness of k_P.

The matrix material is a polymer with graphene oxide randomly oriented reinforcements that are either uniformly or non-uniformly distributed across the thickness of the beam. The modified Halpin–Tsai model is used to evaluate the effective Young's modulus of the GO/polymer nanocomposites in which the GOs are assumed to be circular disk-shaped fillers dispersed in the polymer matrix. The effective Young's modulus of the graphene oxide/polymer composite, E_c, can be calculated as (Weon 2009, Van Es 2001)

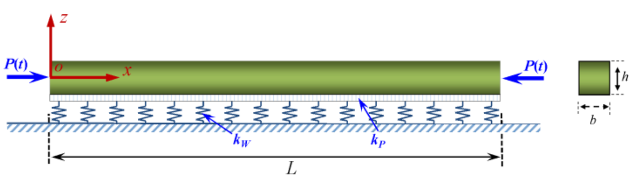

Fig. 1 Schematic of a FG-GORC beam rests on a Winkler–Pasternak elastic substrate

Table 1 Graphene oxide distribution patterns

Distribution pattern	Distribution functions	Υ_i	g_{max}	Schematic
Uniform (UD)	$g(z)=\Upsilon_1 g_{GO}$	1	g_{GO}	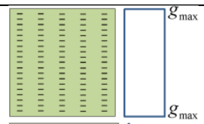
FG-O	$g(z)=\Upsilon_2 g_{GO}\left(1-\frac{2\lvert z\rvert}{h}\right)$	2	$2g_{GO}$	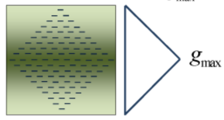
FG-X	$g(z)=\Upsilon_3 g_{GO}\left(\frac{\lvert z\rvert}{h}\right)$	4	$2g_{GO}$	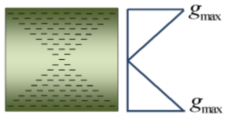
FG-V	$g(z)=\Upsilon_4 g_{GO}\left(1+\frac{2z}{h}\right)$	1	$2g_{GO}$	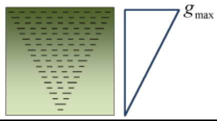

$$E_C = 0.49E_L + 0.51E_T \tag{1}$$

where 0.49 and 0.51 are the parameters representing the reinforcement efficiency of the nanofillers in the longitudinal and transverse directions. These values indicate that the GO nanofillers have almost the same reinforcement efficiencies in the two orthogonal directions. E_L denotes the longitudinal modulus and E_T denotes the transverse modulus given by (Harris 1986)

$$\begin{cases} E_L = \dfrac{1+\xi_L\eta_L V_{GO}}{1-\eta_L V_{GO}} E_M \\ E_T = \dfrac{1+\xi_W\eta_W V_{GO}}{1-\eta_W V_{GO}} E_M \end{cases} \tag{2}$$

Substituting Eq. (2) into Eq. (1) gives

$$E_C = 0.49\frac{1+\xi_L\eta_L V_{GO}}{1-\eta_L V_{GO}} E_M + 0.51\frac{1+\xi_W\eta_W V_{GO}}{1-\eta_W V_{GO}} E_M \tag{3}$$

where

$$\eta_L = \frac{(E_{GO}/E_M)-1}{(E_{GO}/E_M)+\xi_L} \tag{4a}$$

$$\eta_W = \frac{(E_{GO}/E_M)-1}{(E_{GO}/E_M)+\xi_W} \tag{4b}$$

where E_M and E_{GO} denote the Young's moduli of the polymer matrix and the GO, V_{GO} denotes the volume fraction of the GOs, and ξ_L and ξ_W characterize the geometry and size of the GO nanofillers and are defined as (Zhang *et al.* 2018)

$$\xi_L = \xi_W = 2\left(\frac{d_{GO}}{t_{GO}}\right) \tag{5}$$

in which d_{GO} denotes the average diameter and t_{GO} denotes the average thickness of the GO particles. The mass density, ρ_c, and Poisson's ratio, v_c, of the GO/polymer nanocomposite are calculated using the mixture rule as

$$\rho_C = V_{GO}\rho_{GO} + V_M\rho_M \tag{6a}$$

$$v_C = V_{GO}v_{GO} + V_M v_M \tag{6b}$$

where V_M denotes the polymer matrix volume fraction and subscript "GO" denotes the graphene oxide, "*M*" denotes the polymer matrix and "*C*" denotes the GO/polymer nanocomposite. The GO volume fraction is given by

$$V_{GO} = \frac{g_{GO}}{g_{GO} + (\rho_{GO}/\rho_M)(1-g_{GO})} \tag{7}$$

where g_{GO} denotes the total weight fraction of the GOs in the nanocomposite.

As previously mentioned, the GO nanofillers are assumed to be either uniformly or non-uniformly dispersed within the polymer matrix. The current study considers four GO distribution patterns as listed in Table 1.

where Υ_i (i=1, 2, 3 and 4) denote the control coefficients in the GO weight distribution functions with each design having the same total GO weight fraction. g_{max} denotes the maximum weight fraction across the thickness direction for each distribution.

Unless otherwise stated, the graphene oxide dimensions are d_{GO}=15 nm and t_{GO}=0.6 nm. The graphene oxide and epoxy properties are ρ_{GO}=1.09 g/cm^3, E_{GO}=444.8 GPa, ρ_M=1.2 g/cm^3, E_M=3.0 GPa, v_M=0.34, and v_{GO}=0.165 (Zhang *et al.* 2018).

3. Theory and formulations

An accurate, efficient stability model was developed using an improved third order shear deformation theory with modified couple stress theory. The governing equations for the mechanical buckling, free vibrations and dynamic stability of the microbeams were derived using Lagrange's equations and then discretized in matrix form using the Chebyshev-Ritz method.

3.1 Modified couple stress theory

The modified couple stress model (Yang *et al.* 2002) relates the strain energy, U, for a linear elastic material-occupying region, Ω, to the strain and curvature tensors as

$$U = \frac{1}{2}\int_{\Omega}\left(\sigma_{ij}\varepsilon_{ij} + m_{ij}\chi_{ij}\right)d\Omega \tag{8}$$

where i, j =1, 2, 3. σ_{ij} represents the Cauchy stress tensor, ε_{ij} represents the classical strain tensor, m_{ij} is the deviatoric part of the couple stress tensor and χ_{ij} is the symmetric curvature tensor. The strain and curvature tensors are defined as

$$\varepsilon_{ij} = \frac{1}{2}\left(u_{i,j} + u_{j,i}\right) \tag{9a}$$

$$\chi_{ij} = \frac{1}{2}\left(\theta_{i,j} + \theta_{j,i}\right) \tag{9b}$$

where $u_{i,j}$ are the displacement vector components and θ_i are the rotation vector components

$$\theta_i = \frac{1}{2}e_{ijk}u_{k,j} \tag{10}$$

where e_{ijk} is the permutation symbol. The Cauchy stress tensor, σ_{ij}, and the couple stress tensor, m_{ij}, are given by

$$\sigma_{ij} = \lambda\varepsilon_{kk}\delta_{ij} + 2\mu\varepsilon_{ij} \tag{11a}$$

$$m_{ij} = 2\mu l^2\chi_{ij} \tag{11b}$$

where λ and μ are the Láme's constants and δ_{ij} is the Kronecker delta. The Láme's constants are given by

$$\lambda(z) = \frac{\nu(z)E(z)}{\left[1+\nu(z)\right]\left[1-2\nu(z)\right]} \tag{12a}$$

$$\mu(z) = \frac{E(z)}{2\left[1+\nu(z)\right]} \tag{12b}$$

The symbol l in Eq. (11(b)) is a material length scale parameter, which is equal to the square root of the ratio of the modulus of curvature to the modulus of shear and is physically a property measuring the effect of the couple stress (Mindlin 1963, Park and Gao 2006). This parameter can be determined from torsion tests of slim cylinders of various diameters (Chong *et al.* 2001) or bending tests of thin beams of various thicknesses (Park and Gao 2006). Measurements in the literature show that the material length scale parameter is 17.6 μm for homogeneous epoxy beams (Lam *et al* 2003). Due to lack of information for the material length scale parameter of FG-GORCs, l=17.6 μm is also used in the present work.

3.2 Third order shear deformation theory

The improved third-order shear deformation (TSDT) was originally proposed by Shi (2007) based on a kinematics of displacements analysis and has been proved to be more reliable and accurate than other theories (Shi 2007, Wattanasakulpong *et al.* 2011) because the kinematics of displacements theory is derived from elasticity theory rather than the displacement theories used in other approaches. The displacement field given by this third-order shear deformation theory (TSDT) can be expressed as (Shi 2007, Wattanasakulpong *et al.* 2011).

$$\begin{cases} u_x = u_0(x,t) + \frac{5}{4}\left(z - \frac{4}{3h^2}z^3\right)\phi_x(x,t) + \left(\frac{1}{4}z - \frac{5}{3h^2}z^3\right)\frac{\partial w_0(x,t)}{\partial x} \\ u_y = 0 \\ u_z = w_0(x,t) \end{cases} \tag{13}$$

where u_x, u_y and u_z are the x, y and z components of the displacement field at the prescribed point (x,y,z) on a beam cross section at time t, u_0 and w_0 define the generalized displacements at the mid-plane of the beam in the x and z directions and ϕ_x denotes the beam rotation. The non-zero strains and the non-zero components of the symmetric part of the curvature tensor can be expressed from Eqs. (9) and (10) as

$$\begin{cases} \varepsilon_{xx} = \frac{\partial u_0}{\partial x} + \frac{z}{4}\left(5\frac{\partial\phi_x}{\partial x} + \frac{\partial^2 w_0}{\partial x^2}\right) - \frac{5z^3}{3h^2}\left(\frac{\partial\phi_x}{\partial x} + \frac{\partial^2 w_0}{\partial x^2}\right) \\ \varepsilon_{xz} = \frac{5}{4}\left(\phi_x + \frac{\partial w_0}{\partial x}\right) - \frac{5z^2}{h^2}\left(\phi_x + \frac{\partial w_0}{\partial x}\right) \\ \chi_{xy} = \chi_{yx} = \frac{5}{16}\left(\frac{\partial\phi_x}{\partial x} - \frac{3}{5}\frac{\partial^2 w_0}{\partial x^2}\right) - \frac{5z^2}{4h^2}\left(\frac{\partial\phi_x}{\partial x} + \frac{\partial^2 w_0}{\partial x^2}\right) \\ \chi_{yz} = \chi_{zy} = -\frac{5z}{2h^2}\left(\phi_x + \frac{\partial w_0}{\partial x}\right) \end{cases} \tag{14}$$

The classical stress and the couple stress tensor are

$$\begin{cases} \sigma_{xx} = Q_{11}(z)\varepsilon_{xx} \\ \sigma_{xz} = Q_{55}(z)\varepsilon_{xz} \\ m_{xy} = m_{yx} = 2\mu(z)l^2\chi_{xy} \\ m_{yz} = m_{zy} = 2\mu(z)l^2\chi_{yz} \end{cases} \tag{15}$$

where Q_{11}(z) and Q_{55}(z) are the elastic constants which vary continuously through the beam thickness

$$\begin{cases} Q_{11}(z) = \frac{E(z)}{1-\nu^2} \\ Q_{55}(z) = \frac{E(z)}{2(1+\nu)} \\ \mu(z) = \frac{E(z)}{2(1+\nu)} \end{cases} \tag{16}$$

The strain energy, U, of the beam is given as

$$U = \frac{1}{2}\int_0^L\int_{-h/2}^{h/2} b\left(\sigma_{xx}\varepsilon_{xx} + \sigma_{xz}\varepsilon_{xz} + 2m_{xy}\chi_{xy} + 2m_{yz}\chi_{yz}\right)\mathrm{d}z\mathrm{d}x \tag{16}$$

Substituting Eqs. (13)-(16) into Eq. (17) gives the strain energy expression as a function of the material stiffness and strain components

$$U=\frac{1}{2}\int_0^L\left\{\begin{array}{l}A_{11}\left(\frac{\partial u_0}{\partial x}\right)^2+\frac{B_{11}}{2}\left(5\frac{\partial u_0}{\partial x}\frac{\partial \phi_x}{\partial x}+\frac{\partial u_0}{\partial x}\frac{\partial^2 w_0}{\partial x^2}\right)+\frac{D_{11}}{16}\left(5\frac{\partial \phi_x}{\partial x}+\frac{\partial^2 w_0}{\partial x^2}\right)^2-\frac{10E_{11}}{3h^2}\left(\frac{\partial u_0}{\partial x}\frac{\partial \phi_x}{\partial x}+\frac{\partial u_0}{\partial x}\frac{\partial^2 w_0}{\partial x^2}\right)\\ -\frac{5F_{11}}{6h^2}\left[5\left(\frac{\partial \phi_x}{\partial x}\right)^2+6\frac{\partial \phi_x}{\partial x}\frac{\partial^2 w_0}{\partial x^2}+\left(\frac{\partial^2 w_0}{\partial x^2}\right)^2\right]+\frac{25H_{11}}{9h^4}\left(\frac{\partial \phi_x}{\partial x}+\frac{\partial^2 w_0}{\partial x^2}\right)^2+\frac{25A_{55}}{16}\left(\phi_x+\frac{\partial w_0}{\partial x}\right)^2\\ -\frac{25D_{55}}{2h^2}\left(\phi_x+\frac{\partial w_0}{\partial x}\right)^2+\frac{25F_{55}}{h^4}\left(\phi_x+\frac{\partial w_0}{\partial x}\right)^2+\frac{25M_{55}}{64}\left(\frac{\partial \phi_x}{\partial x}-\frac{3}{5}\frac{\partial^2 w_0}{\partial x^2}\right)^2+\frac{25N_{55}}{h^4}\left(\phi_x+\frac{\partial w_0}{\partial x}\right)^2\\ -\frac{N_{55}}{8h^2}\left[5\left(\frac{\partial \phi_x}{\partial x}\right)^2+3\left(\frac{\partial^2 w_0}{\partial x^2}\right)^2+2\frac{\partial \phi_x}{\partial x}\frac{\partial^2 w_0}{\partial x^2}\right]+\frac{25S_{55}}{4h^4}\left(\frac{\partial \phi_x}{\partial x}+\frac{\partial^2 w_0}{\partial x^2}\right)^2\end{array}\right\}\mathrm{d}x \tag{18}$$

where A_{11}, B_{11}, D_{11}, F_{11}, H_{11}, A_{55}, D_{55}, F_{55}, M_{55}, N_{55} and S_{55} are the material stiffness constants defined as

$$\begin{cases}(A_{11},B_{11},D_{11},E_{11},F_{11},H_{11})=b\int_{-h/2}^{h/2}Q_{11}(z)\left(1,z,z^2,z^3,z^4,z^6\right)\mathrm{d}z\\ (A_{55},D_{55},F_{55})=b\int_{-h/2}^{h/2}Q_{55}(z)\left(1,z^2,z^4\right)\mathrm{d}z\\ (M_{55},N_{55},S_{55})=b\int_{-h/2}^{h/2}\mu(z)l^2\left(1,z^2,z^4\right)\mathrm{d}z\end{cases} \tag{19}$$

The kinetic energy of FG-GORC microbeam is

$$T=\frac{1}{2}\int_0^L\int_{-h/2}^{h/2}b\left\{\rho(z)\left[\left(\frac{\partial u}{\partial t}\right)^2+\left(\frac{\partial w}{\partial t}\right)^2\right]\right\}\mathrm{d}z\mathrm{d}x \tag{20}$$

where ρ (z) is the mass density of the beam which varies in the thickness direction.

Substituting Eq. (13) into Eq. (20) gives the kinetic energy as

$$T=\frac{1}{2}\int_0^L\left\{\begin{array}{l}I_0\left[\left(\frac{\partial u_0}{\partial t}\right)^2+\left(\frac{\partial w_0}{\partial t}\right)^2\right]+\frac{I_1}{2}\left(5\frac{\partial u_0}{\partial t}\frac{\partial \phi_x}{\partial t}+\frac{\partial u_0}{\partial t}\frac{\partial^2 w_0}{\partial x\partial t}\right)\\ +\frac{I_2}{16}\left[25\left(\frac{\partial \phi_x}{\partial t}\right)^2+10\frac{\partial \phi_x}{\partial t}\frac{\partial^2 w_0}{\partial x\partial t}+\left(\frac{\partial^2 w_0}{\partial x\partial t}\right)^2\right]\\ -\frac{10I_3}{3h^2}\left(\frac{\partial u_0}{\partial t}\frac{\partial \phi_x}{\partial t}+\frac{\partial u_0}{\partial t}\frac{\partial^2 w_0}{\partial x\partial t}\right)\\ -\frac{5I_4}{6h^2}\left[5\left(\frac{\partial \phi_x}{\partial t}\right)^2+6\frac{\partial \phi_x}{\partial t}\frac{\partial^2 w_0}{\partial x\partial t}+\left(\frac{\partial^2 w_0}{\partial x\partial t}\right)^2\right]\\ +\frac{25I_6}{9h^4}\left[\left(\frac{\partial \phi_x}{\partial t}\right)^2+2\frac{\partial \phi_x}{\partial t}\frac{\partial^2 w_0}{\partial x\partial t}+\left(\frac{\partial^2 w_0}{\partial x\partial t}\right)^2\right]\end{array}\right\}\mathrm{d}x \tag{21}$$

where $I_i=b\int_{-h/2}^{h/2}\rho(\mathrm{z})z^{\mathrm{i}},\quad i=0,1,2,3,4,6$ are the inertia terms.

The work done by the axial force, $P(t)$, is

$$W_{\mathrm{axial}}=\frac{1}{2}\int_0^L\left[P(t)\left(\frac{\partial w}{\partial x}\right)^2\right]\mathrm{d}x \tag{22}$$

The lower surface of the FG-GORC microbeam is assumed to rest on a Winkler–Pasternak elastic substrate that has two elastic stiffness parameters, k_W and k_P. The work done by the elastic substrate is

$$W_{\mathrm{sub}}=-\int_0^L\left[\left(k_W w-k_P\frac{\partial^2 w}{\partial x^2}\right)w\right]\mathrm{d}x \tag{23}$$

The total energy functional, Π, is then

$$\Pi=U-T-W_{\mathrm{axial}}-W_{\mathrm{sub}} \tag{24}$$

3.3 Solution method

The Ritz method is an effective tool for analyzing the structural behavior of beams. Since the functions depend only on the essential type of boundary conditions (Reddy 2003), various functions can be used as admissible functions. The present work uses Chebyshev polynomials as the admissible functions.

Each of the displacement amplitude functions in Eq. (13) can be written as three Chebyshev polynomials multiplied by a boundary function, which ensures that the displacement component satisfies the essential geometric boundary conditions

$$\begin{cases}u_0(x,t)=B_u(x)\sum_{i=1}^{N}U_i(t)P_i(x)\\ w_0(x,t)=B_w(x)\sum_{i=1}^{N}W_i(t)P_i(x)\\ \phi_x(x,t)=B_\phi(x)\sum_{i=1}^{N}V_i(t)P_i(x)\end{cases} \tag{25}$$

B_Ξ (x) (Ξ=u, w and ϕ) are the boundary functions. $P_i(x)$ is the i^{th} Chebyshev polynomial of the first kind, which is commonly known as "the most optimal expansion" (Chen and Zhang 2017, Liang *et al.* 2018) and is defined in the interval [−1, 1] as

$$P_i(x)=\cos\left((i-1)\arccos\left(\frac{2x}{L}-1\right)\right),\quad i=1,2,3... \tag{26}$$

The recursive relationship is

$$\begin{cases}P_0(\chi)=1\\ P_1(\chi)=\chi\\ P_{i+1}(\chi)=2\chi P_i(\chi)-P_{i-1}(\chi)\end{cases} \tag{27}$$

Chebyshev polynomials have two distinct advantages as admissible functions for each displacement component (Fox and Parker 1968, Zhou *et al*. 2006). One is that $P_i(x)$ is a complete, orthogonal series in the interval [−1, 1] and has more rapid convergence and better numerical stability in computations than other polynomials. The other advantage is that $P_i(x)$ can be expressed as simple cosine functions as shown in Eq. (26) which reduces the coding effort. The boundary functions $B_\Xi(x)$ ($\Xi=u$, w and ϕ) corresponding to u, w and ϕ_x are given by

$$B_\Xi(x)=\left(\frac{x}{L}\right)^{L_\Xi}\left(1-\frac{x}{L}\right)^{R_\Xi} \tag{28}$$

where L_Ξ and R_Ξ are indices from the essential geometric boundary conditions:

1) Hinged-Hinged (H-H)

x=0: u_0=0; w=0; $\phi_x\neq0$

x=L: u_0=0; w=0; $\phi_x\neq0$

2) Clamped-Clamped (C-C)

x=0: u_0=0; w=0; $\frac{dw}{dx}=0$; $\phi_x\neq0$

x=L: u_0=0; w=0; $\frac{dw}{dx}=0$; $\phi_x\neq0$

3) Clamped-Hinged (C-H)

x=0: u_0=0; w=0; $\frac{dw}{dx}=0$; $\phi_x=0$

x=L: u_0=0; w=0; $\phi_x\neq0$

4) Clamped-Free (C-F)

x=0: u_0=0; w=0; $\frac{dw}{dx}=0$; $\phi_x=0$

x=L: $u_0\neq0$; $w\neq0$; $\frac{dw}{dx}\neq0$; $\phi_x\neq0$

Table 2 lists the indices for the various boundary conditions.

Lagrange's equations are used to derive the governing equations for the vibration and dynamic stability of the FG-GORC microbeams

$$\frac{d}{dt}\left(\frac{\partial\Pi}{\partial\dot{q}_i}\right)+\frac{\partial\Pi}{\partial q_i}=0 \tag{29}$$

where q_i represents the unknown coefficients, $U_i(t)$, $W_i(t)$and $V_i(t)$, and the over-dot denotes the partial derivative with respect to time. The equation of motion is then

$$[\boldsymbol{M}]\ddot{\boldsymbol{q}}+\left\{[\boldsymbol{K}]-[\boldsymbol{K}]_{\text{sub}}-P(t)[\boldsymbol{K}]_{\text{axial}}\right\}\boldsymbol{q}=0 \tag{30}$$

Table 2 Various boundary conditions indices

Boundary conditions	L_u	L_φ	L_w	R_u	R_φ	R_w
H-H	1	0	1	1	0	1
C-C	1	1	2	1	1	2
C-H	1	1	2	1	0	1
C-F	1	1	2	0	0	0

where $[\boldsymbol{M}]$ denotes the mass matrix, $[\boldsymbol{K}]$ denotes the structural stiffness matrix, $[\boldsymbol{K}]_{\text{sub}}$ is the additional stiffness matrix generated by the elastic foundation, and $[\boldsymbol{K}]_{\text{axial}}$ is the geometric stiffness matrix produced by the axial force.

If the axial force is time-independent and neglecting the inertia term in Eq. (30) leads to the equation for the static buckling

$$\left\{[\boldsymbol{K}]-[\boldsymbol{K}]_{\text{sub}}-P_{cr}[\boldsymbol{K}]_{\text{axial}}\right\}\boldsymbol{q}_{\text{cr}}=0 \tag{31}$$

where P_{cr} represents the critical buckling load for the microbeam and $\boldsymbol{q}_{\text{cr}}$ denotes the eigenvector from the displacement functions that represents the buckling mode shapes of the structures.

For free vibrations of the microbeam resting on the elastic substrate, the unknown coefficients $(\bar{U}_n,\bar{W}_n,\bar{V}_n)$ can be written in a harmonic form as: $(U_n,W_n,V_n)=(\bar{U}_n,\bar{W}_n,\bar{V}_n)e^{i\omega_n t}$, $i=\sqrt{-1}$, where ω_n denotes the vibration frequencies. In addition, the axial force is removed in the vibration analysis. Thus, the governing equation for the free vibrations of the beam derived from Eq. (30) is

$$\left\{\left([\boldsymbol{K}]-[\boldsymbol{K}]_{\text{sub}}\right)-\omega^2[\boldsymbol{M}]\right\}\boldsymbol{q}_{\text{vib}}=0 \tag{32}$$

where $\boldsymbol{q}_{\text{vib}}$ denotes the eigenvectors from the displacement functions that represent the modal shapes of the structures.

For the dynamic stability, the periodic axial force can be expressed as

$$P(t)=P_s+P_d\cos(\vartheta t) \tag{33}$$

where P_s and P_d are the static and dynamic force components and ϑ is the excitation frequency of the periodic axial force. Substituting Eq. (33) into Eq. (30) gives a Mathieu-Hill type equation for the dynamic stability of FG-GORC microbeams subjected to a periodic axial force while resting on the elastic substrate

$$[\boldsymbol{M}]\ddot{\boldsymbol{q}}+\left\{[\boldsymbol{K}]-[\boldsymbol{K}]_{\text{sub}}-\left[P_s+P_d\cos(\vartheta t)\right][\boldsymbol{K}]_{\text{axial}}\right\}\boldsymbol{q}=0 \tag{34}$$

The instabilities occur only within certain regions of the frequency-driving amplitude plane. The boundaries of the unstable regions on this plane represent the periodic solutions of the equations of motion. The unstable region is separated from the stable region by periodic solutions with periods of T_0 and $2T_0$, where $T_0=2\pi/\vartheta$. The solutions with period 2T have greater practical importance because they are associated with the principle unstable regions that are usually much larger than the secondary unstable regions defined by the solutions with period T_0. The periodic solutions with period $2T_0$ can be found using Bolotin's first approximation (Bolotin 1964) as a first order approximation of the equations. The periodic solution of Eq. (30) with period $2T_0$ takes the form of a trigonometric series

$$\boldsymbol{q}=\sum_{k=1,3,\cdots}^{\infty}\left[\boldsymbol{a}_k\sin\frac{k\vartheta t}{2}+\boldsymbol{b}_k\cos\frac{k\vartheta t}{2}\right] \tag{35}$$

Table 3 Convergence and validation for free vibration of an isotropic beam resting on an elastic foundation (L/h=15)

N	(k_W, k_P/π^2)=(0, 0)				(k_W, k_P/π^2)=(10^2, 0)			(k_W, k_P/π^2)=(10^2, 1)		
	$\bar{P}_{cr}$	1st order	2nd order	3rd order	1st order	2nd order	3rd order	1st order	2nd order	3rd order
5	0.36161	3.1300	6.2065	9.2428	3.7399	6.3072	9.2735	4.1362	6.6600	9.5325
6	0.36142	3.1299	6.1940	9.2104	3.7398	6.2953	9.2414	4.1361	6.6496	9.5022
7	0.36142	3.1299	6.1940	9.1413	3.7398	6.2953	9.1730	4.1361	6.6495	9.4378
8	0.36142	3.1299	6.1939	9.1404	3.7398	6.2952	9.1721	4.1361	6.6495	9.4369
9	0.36142	3.1299	6.1939	9.1393	3.7398	6.2952	9.1711	4.1361	6.6495	9.4360
10	0.36142	3.1299	6.1939	9.1393	3.7398	6.2952	9.1711	4.1361	6.6495	9.4360
Chen (2004)		3.1302472			3.7389477			4.1347188		

Table 4 Critical buckling loads of the functionally graded microbeams

L/h	E_2/E_1	C-F		H-H		C-C	
		Ke *et al.*(2009)	Present	Ke *et al.*(2009)	Present	Ke *et al.*(2009)	Present
6	0.2	0.002518	0.002460	0.010851	0.010815	0.03111	0.03085
	1.0	0.005740	0.005597	0.021117	0.021120	0.06884	0.06891
	5.0	0.012588	0.012300	0.054256	0.054076	0.15554	0.15425
16	0.2	0.0003526	0.0003515	0.001636	0.001635	0.005418	0.005410
	1.0	0.0008015	0.0008009	0.003176	0.003176	0.01227	0.01229
	5.0	0.001762	0.001757	0.008179	0.008175	0.02709	0.02705

where $\boldsymbol{a}_k$ and $\mathbf{b}_k$ are arbitrary constant vectors. The solution of the first order approximation with k=1 provides acceptable accuracy and conservative results of the first unstable region, especially for periodic axial loading with one excitation frequency (Bolotin 1964, Xin *et al.* 2011). Thus, the fundamental unstable region is sought.

Differentiating a one-term solution twice with respect to time t gives

$$\ddot{\boldsymbol{q}} = -\frac{\vartheta^2}{4}\boldsymbol{a}_1 \sin\frac{\vartheta t}{2} - \frac{\vartheta^2}{4}\boldsymbol{b}_1 \cos\frac{\vartheta t}{2} \tag{36}$$

Substituting the $\boldsymbol{q}$ and $\ddot{\boldsymbol{q}}$ into Eq. (30), simplifying the trigonometric relations and then comparing the coefficients of $\sin\frac{\vartheta t}{2}$ and $\cos\frac{\vartheta t}{2}$ gives two algebraic matrix equations for $\boldsymbol{a}_1$ and $\boldsymbol{b}_1$

$$\left\{[\boldsymbol{K}]-[\boldsymbol{K}]_{\text{sub}}-\left(P_s-\frac{P_d}{2}\right)[\boldsymbol{K}]_{\text{axial}}-\frac{\vartheta^2}{4}[\boldsymbol{M}]\right\}\boldsymbol{a}_1=0 \tag{37a}$$

$$\left\{[\boldsymbol{K}]-[\boldsymbol{K}]_{\text{sub}}-\left(P_s+\frac{P_d}{2}\right)[\boldsymbol{K}]_{\text{axial}}-\frac{\vartheta^2}{4}[\boldsymbol{M}]\right\}\boldsymbol{b}_1=0 \tag{37b}$$

The following relations were used to simplify the trigonometric relations

$$\cos\vartheta t\cos\frac{\vartheta t}{2}=\frac{1}{2}\left(\cos\frac{\vartheta t}{2}+\cos\frac{3\vartheta t}{2}\right) \tag{38a}$$

$$\cos\vartheta t\cos\frac{\vartheta t}{2}=\frac{1}{2}\left(-\sin\frac{\vartheta t}{2}+\sin\frac{3\vartheta t}{2}\right) \tag{38b}$$

The excitation frequencies, ϑ, can be determined from Eq. (37) for a given dynamic force P_d using standard eigenvalue algorithms. The variation of the eigenvalue ϑ with respect to P_d can be plotted with the ϑ- P_d plane showing the unstable regions for the FG-GORC microbeams subjected to a periodic axial load while resting on the elastic substrate. The intersection at P_d =0 represents the origin of the principle unstable region.

4. Convergence and validation studies

The validity and accuracy of the model were verified by comparing the results for several numerical examples with data in the literature.

Increasing N in Eq. (25) leads to results that are more accurate but will require more computational time; thus, a suitable value of N needs to be determined for a balance between the accuracy and the computational complexity in the solution procedure. A simply-supported isotropic beam with Poisson's ratio of 0.3 (ν=0.3) is considered as an illustration for the convergence and validation. The dimensionless critical buckling load ($\bar{P}_{cr}=\frac{P_{cr}}{EA}$) of the beam without an elastic foundation and the first three dimensionless natural frequencies ($\bar{\omega}_i^2=\omega_i L^2\sqrt{\frac{\rho A}{EI}}$) of the beam resting on the elastic foundation were calculated and

Table 5 Size effect on the dimensionless fundamental frequencies for SiC/Al beams (L/h=5)

BCs	h/l	k=0 Trinh *et al.* (2018)	k=0 Present	k=1 Trinh *et al.* (2018)	k=1 Present	k=10 Trinh *et al.* (2018)	k=10 Present
HH	1	15.7140	15.7140	12.1506	12.1507	8.1733	8.1734
	5	6.8405	6.8405	5.2905	5.2905	3.9046	3.9046
	∞	6.2009	6.2008	4.7944	4.7943	3.6022	3.6022
CC	1	33.5290	33.5321	25.7024	25.7056	17.4627	17.4672
	5	13.8093	13.8112	10.2076	10.2104	7.3016	7.3027
	∞	12.2556	12.2713	8.9576	8.9692	6.3403	6.3614
CH	1	18.1099	18.1099	14.2757	14.2677	9.4339	9.4285
	5	10.2151	10.1005	7.4889	7.4897	5.4437	5.4197
	∞	9.1925	9.1739	6.6568	6.6641	4.9064	4.8755
CF	1	5.6973	5.6986	4.3504	4.3519	2.9127	2.9135
	5	2.5043	2.5051	1.8236	1.8243	1.3667	1.3678
	∞	2.2769	2.2762	1.6362	1.6360	1.2604	1.2599

Table 6 Dimensionless critical buckling loads for FG-GORC beams (Hinged-Hinged)

L/h	FGX Zhang *et al.* (2018)	FGX Present	FGO Zhang *et al.* (2018)	FGO Present	UD Zhang *et al.* (2018)	UD Present
10	0.0116	0.0115	0.0086	0.0086	0.0101	0.0101
15	0.0052	0.0052	0.0039	0.0039	0.0046	0.0046
20	0.0030	0.0030	0.0022	0.0022	0.0026	0.0026

Table 7 Dimensionless fundamental frequencies of FG-GORC beams (Hinged-Hinged)

L/h	FGX Zhang *et al.* (2018)	FGX Present	FGO Zhang *et al.* (2018)	FGO Present	UD Zhang *et al.* (2018)	UD Present
10	0.3379	0.3363	0.2921	0.2910	0.3159	0.3147
15	0.2271	0.2267	0.1959	0.1955	0.2121	0.2118
20	0.1708	0.1707	0.1473	0.1471	0.1595	0.1594

compared with those from Chen's work (2004). The comparisons in Table 3 show excellent agreement. In addition, N=7 was found to be large enough to obtain accurate results for Eq. (25).

The dimensionless critical buckling loads of a functionally graded microbeam with the materials properties following an exponential variation through the thickness direction are compared with those of Ke *et al*. (2009) in Table 4 for three boundary conditions. The beam thickness h=0.1 m, the slenderness ratio L/h=6 or 16, the Young's modulus ratio E_2/E_1= 0.2, 1.0 or 5.0, E_1 = 70 GPa, and ν_1 = 0.33. The present results agree very well with the results of Ke *et al*. (2009)

The size effect on the vibration behavior of the functionally graded microbeam was also examined using the present model. The functionally graded microbeam was made of SiC (E_c=427 GPa, ρ_c=3100 kg/m^3, υ_c=0.17) and Al (E_m=70 GPa, ρ_m=2702 kg/m^3, υ_m=0.3). The length scale paramter, l, was set to 15 μm. The elastic properties of the functionally graded microbeam were evaluated using

$$M(z)=(M_c-M_m)\left(\frac{1}{2}+\frac{z}{h}\right)^k+M_m \tag{39}$$

where M_δ represents the mechanical properties (E, ρ, υ) of the two constituents of the functionally graded microbeam. The subscript, δ, represent 'c' and 'm' for the ceramic and the metal. k is the power-law index. Table 5 compares the dimensionless fundamental frequencies ($\bar{\Omega}=\frac{\omega L^2}{h}\sqrt{\frac{\rho_m}{E_m}}$) of the functionally graded microbeam subjected to various boundary conditions (BCs) calculated using the present method to the results of Luan *et al.* (2018) which were based on higher-order beam deformation theories. The present results again agree well with the previous data for microbeams.

Tables 6 and 7 compares the predicted dimensionless critical buckling loads and fundamental frequencies of 22-layered FG-GORC laminated microbeams with the results

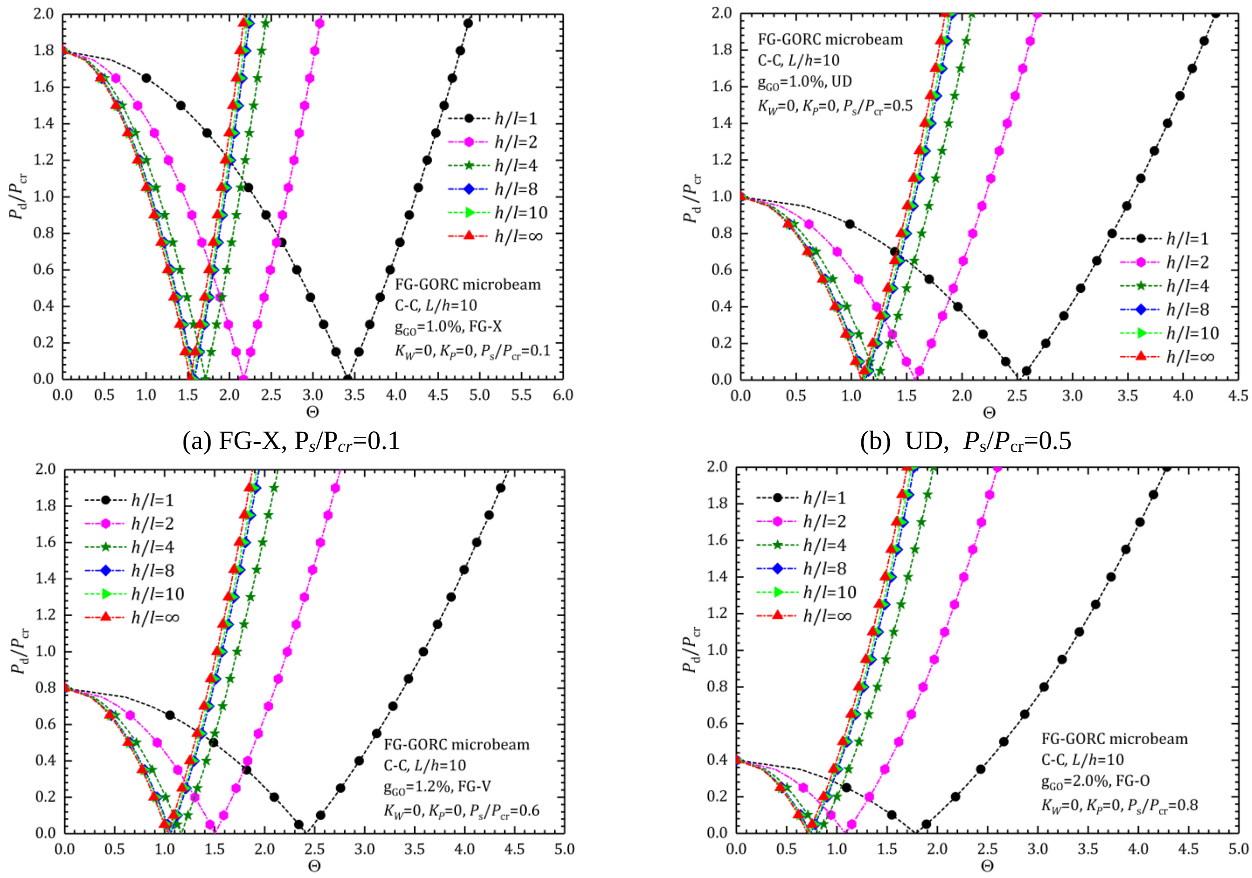

(a) FG-X, P_s/P_{cr}=0.1 (b) UD, P_s/P_{cr}=0.5

(c) FG-V, P_s/P_{cr}=0.6 (d) FG-O, P_s/P_{cr}=0.8

Fig. 2 Effects of the microbeam size on the unstable region of the FG-GORC microbeam

of Zhang *et al*. (2018). The multilayer beam with 22 or more layers is an excellent approximation of an ideal functionally graded beam structure with a continuous, smooth variation of both the material composition and the properties. The total GO weight fraction was g_{GO}=0.3% and the functionally graded material properties of the beam were controlled by the volume variation of GOs in each layer. Three types of GO distributions were considered. Tables 6 and 7 show a good agreement between the results.

5. Numerical examples and discussion

The model is used here to investigate the dynamic stability characteristics of functionally graded graphene oxide reinforced composite (FG-GORC) microbeams subjected to a periodic axial force while resting on an elastic substrate. Some dimensionless parameters are introduced to facilitate the presentation:

Dimensionless excitation frequency:

$$\Theta = \vartheta L\sqrt{\frac{\rho_M}{E_M}}$$

Dimensionless elastic constants of the two-parameter substrate:

$$K_W = \frac{k_w L^4}{E_M I},\quad K_P = \frac{k_p L^4}{E_M I}$$

where I is defined as $I = \dfrac{bh^3}{12}$ and E_M and ρ_M are the Young's modulus and mass density of the pure polymer matrix.

The dynamic stability of FG-GORC microbeams with a periodic axial force was investigated for a wide range of parameters. The variations of the principle unstable regions, as indicated by the ratio of the dynamic axial force, P_d, to the critical buckling load, P_{cr}, are given as functions of the dimensionless excitation frequency, Θ. Fig. 2 shows the effect of the dimensionless length, h/l, on the unstable region for C-C FG-GORC microbeams with the various GO distribution patterns for a microbeam with slenderness ratio of 10. Increasing h/l shifts the unstable region origin to lower excitation frequencies and reduces the width of the unstable region. In addition, the results show that the unstable region is significantly affected for h/l less than 8, which indicates that the size has more influence on the unstable region size for thin microbeams than for thick ones. That is because as h/l increases the proportion of additional structural stiffness due to small scale in total structural stiffness [**K**] descends gradually and become invisible when h/l ≥8. The effects of the boundary conditions on the dynamic stability of the FG-GORC microbeams are shown in Fig. 3. The clamped-clamped end supports again produce the highest excitation frequencies and widest unstable regions for the composite microbeams while the clamped-free ends generate the lowest Θ and the narrowest unstable regions.

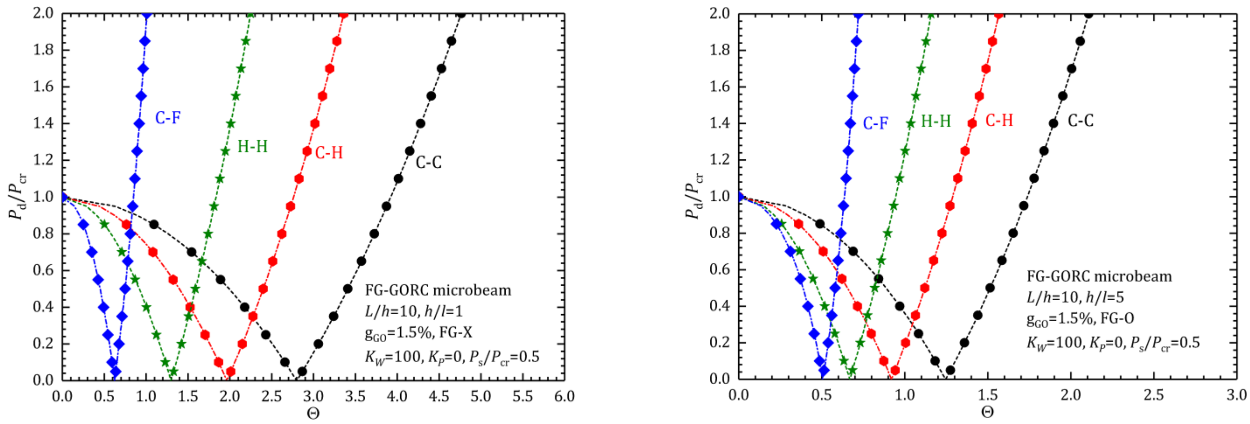

(a) FG-X h/l=1 (b) FG-O h/l=5

Fig. 3 Effects of the boundary conditions on the unstable region of the FG-GORC microbeam

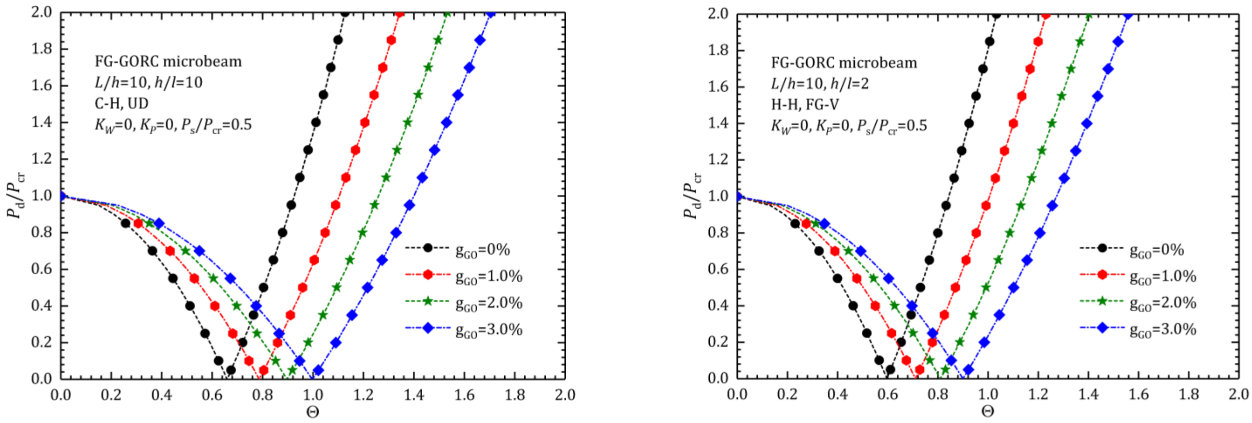

(a) C-H, UD (b)C-H, FG-V

Fig. 4 Effects of the GO weight fraction on the dynamic stability of FG-GORC microbeams

The physical reason for this result is that the clamped-clamped ends provide the most rigorous boundary restrains and produce greatest stiffness of the system. Conversely, the clamped-free ends lead to the smallest stiffness.

Fig. 4 shows the principal unstable regions for the FG-GORC microbeams for various weight fractions. One can observe that additions of GO nanofillers broaden the unstable regions and increase the critical excitation frequencies of the axial load. It is a predictable result since GO nanofillers have extremely high modulus of elasticity compared to polymer matrix, a small amount of GOs can provide remarkable improvements to stiffness and hardness of microbeams,, resulting in higher vibration frequencies.

The influence of GO distribution patterns on the dynamic stability of the FG-GORC microbeams is shown in Fig. 5. It is seen that the FG-X distribution pattern gives the highest origin and the widest unstable region. The results also show that the composite microbeam with the FG-X distribution pattern becomes unstable at higher excitation frequencies than the beams with the other distribution patterns since microbeams with the FG-X distribution have much higher bending resistance to bending deformation. This result demonstrates that the FG-X GO distribution in which the top and bottom surfaces have the highest GO nanofiller content has the highest resistance to bending because such patterns have more GO particles in the top and bottom layers with the highest normal bending stresses which produces the best reinforcement.

The effects of the GO shape as indicated by the particle diameter-to-thickness ratio (d_{GO}/t_{GO}) on the dynamic stability of the FG-GORC microbeams are shown in Fig. 6. In these cases, the GO particle thickness was fixed. The results show that d_{GO}/t_{GO} greatly influences the dynamic stability of FG-GORC microbeams with larger d_{GO}/t_{GO} moving the unstable region origin to higher excitation frequencies and increasing the unstable region width. The curves become much closer at higher d_{GO}/t_{GO} which suggests that the effect of d_{GO}/t_{GO} on the dynamic stability of FG-GORC microbeams is much less at larger diameter-to-thickness ratios. In other words, larger sized GOs are better reinforcing nanofillers than their counterparts with a smaller size, because larger sized nanofillers can provide larger contact surface with polymer matrix and better load transfer from matrix to GOs, being generally beneficial in improving the mechanical properties of the composites. The effects of Winkler and Pasternak foundations on the dynamic stability of FG-GORC microbeams are shown in Figs. 7(a) and 7(b). It is observed that the unstable region not only becomes wider but also moves to the right as both K_W and K_P increase. This is because increasing either of the Winkler and Pasternak foundation parameters increases the

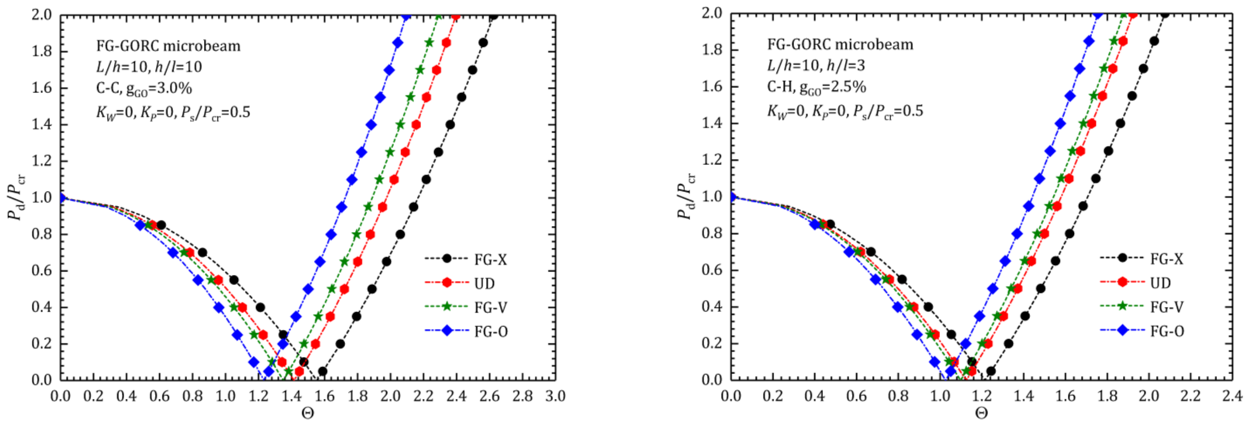

(a) C-C (b) C-H

Fig. 5 Effects of the GO distribution on the dynamic stability of FG-GORC microbeams

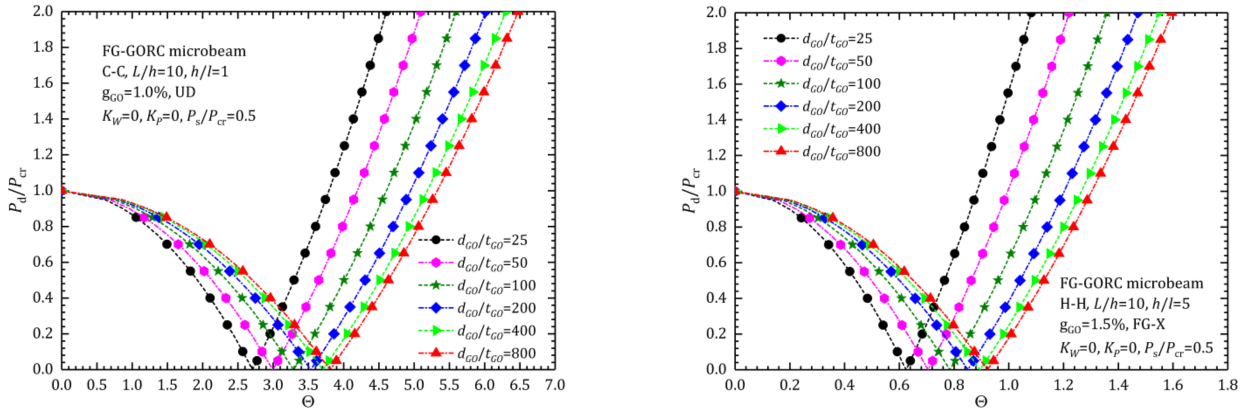

(a) C-C (b) H-H

Fig. 6 Effects of the particle diameter-to-thickness ratio (d_{GO}/t_{GO}) on the principal unstable region of the FG-GORC microbeams

system stiffness, which then increases the critical frequencies.

In addition, From Fig. 7 it is found that with the same increments, the improvement of excitation frequencies resulting from K_W is less than that from K_P, and the variation of width of unstable regions due to K_W varying is not so evident compared with that due to K_P varying. This phenomenon indicates that the location and size of the unstable region are not sensitive to the Winkler foundation with the unstable region only moving slightly to the right as K_W increases, and the Pasternak elastic foundation has a much larger effect on the dynamic stability of the composite microbeam.

6. Conclusions

The current study investigated the dynamic stability of a FG-GORC microbeam subjected to a periodic axial force while resting on an elastic substrate. The GO nanofiller weight fraction was assumed to be graded across the microbeam thickness. The effective Young's modulus of the functionally graded GO reinforced composite (FG-GORC) was determined using the modified Halpin–Tsai model, while the mixture rule was used to evaluate the effective Poisson's ratio and mass density.

A third order shear deformation theory (TSDT) model was used in conjunction with a modified couple stress theory to develop an accurate, efficient model to predict the dynamic stability of this composite microbeam. The Chebyshev polynomial-based Ritz method was used to describe the various immovable boundary conditions of the beam. Lagrange's equations were used to derive the Mathieu-Hill equations for the dynamic stability of the FG-GORC microbeam which were then solved using Bolotin's method. The solution then gave the principal unstable region of the FG-GORC microbeam.

(1) A parametric study showed the effects of the GO particles including their weight fraction, distribution pattern, geometric parameters, and size and the effects of the elastic substrate on the dynamic stability of the microbeam. The main conclusions are:
(2) Adding even a small GO nanofiller mass fraction significantly improves the polymer composite beam stiffness that broadens the unstable regions of the FG-GORC microbeams and increases the allowable excitation frequencies of the periodic axial load. The effects are greater with more GO nanofiller near the top and bottom surfaces of the beam.

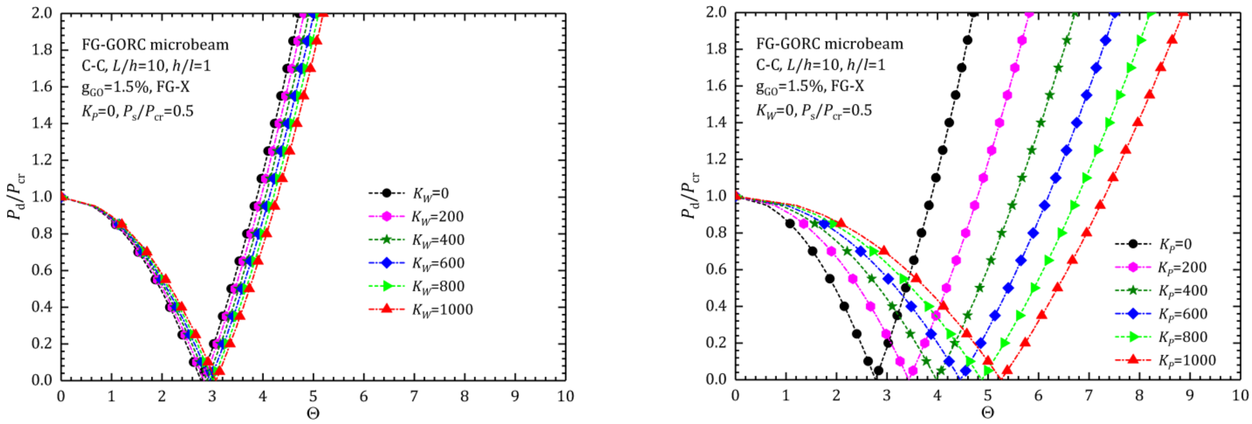

(a) K_P=0, K_W varying (b) K_W =0, K_P varying

Fig. 7 Effects of the elastic substrate on dynamic stability of FG-GORC microbeams

(3) The microbeam size significantly affects the dynamic stability of thin FG-GORC microbeams with less effect for thick microbeams. Reducing the dimensionless length scale, *h*/*l*, significantly increases the critical buckling loads and fundamental frequencies of FG-GORC microbeams.

(4) The GO particle diameter-to-thickness ratio also strongly influences the dynamic stability behaviors of FG-GORC microbeams for diameter-to-thickness ratios less than 400. Increasing the diameter-to-thickness ratio shifts the unstable region origin to higher excitation frequencies and increases the unstable region width.

Increase in the elastic stiffness of the foundation increases the critical excitation frequency and increases the unstable region width. The Pasternak elastic foundation has a greater impact on the mechanical behavior of the FG-GORC microbeam than the Winkler foundation.

Acknowledgments

This study was supported by the National Key Research and Development Program of China (No. 2016YFC0802500), the National Natural Science Foundation of China (No. 51976097), the Science Fund for Creative Research of Groups of NSFC (No. 51621062), and the China Postdoctoral Science Foundation (2018M641333). We thank Prof. D.M. Christopher for editing the English.

References

Arani, A.G. and Kiani, F. (2018), "Nonlinear free and forced vibration analysis of microbeams resting on the nonlinear orthotropic visco-Pasternak foundation with different boundary conditions", *Steel Compos. Struct.*, **28**(2), 149-165. http://dx.doi.org/10.12989/scs.2018.28.2.149.

Arefi, M., Bidgoli, E.M.R., Dimitri, R. and Tornabene, F. (2018), "Free vibrations of functionally graded polymer composite nanoplates reinforced with graphene nanoplatelets", *Aerosp. Sci. Technol.*, **81**, 108-117. https://doi.org/10.1016/j.ast.2018.07.036.

Ashrafi, B., Hubert, P. and Vengallatore S. (2006), "Carbon nanotube-reinforced composites as structural materials for microactuators in microelectromechanical systems", *Nanotechnology*, **17**(19), 4895. https://doi.org/10.1088/0957-4484/17/19/019.

Bolotin, V.V. (1964), *The Dynamic Stability of Elastic Systems*, Holden-Day, San Francisco, CA, USA.

Chen, L. and Zhang, W.P. (2017), "Chebyshev polynomials and their some interesting applications", *Adv. Differ. Equ.* **2017**, 303. https://doi.org/10.1186/s13662-017-1365-1.

Chen, X. Lu, Y. and Li, Y. (2019), "Free vibration, buckling and dynamic stability of bi-directional FG microbeam with a variable length scale parameter embedded in elastic medium", *Appl. Math. Model.*, 67, 430-448. https://doi.org/10.1016/j.apm.2018.11.004.

Chen,W.Q., Lü, C.F. and Bian, Z.G. (2004), "A mixed method for bending and free vibration of beams resting on a Pasternak elastic foundation", *Appl. Math. Model.*, **28**(10), 877-890. https://doi.org/10.1016/j.apm.2004.04.001.

Chong, A.C.M., Yang, F. and Lam, D.C.C. (2001), "Torsion and bending of micron-scaled structures", *J. Mater. Res.*, **16**, 1052-1058. https://doi.org/10.1557/JMR.2001.0146.

Ebrahimi, F. and Barati, M.R. (2016a), "Small-scale effects on hygro-thermo-mechanical vibration of temperature-dependent nonhomogeneous nanoscale beams", *Mech. Adv. Mater. Struct.*, **24**(11), 924-936. https://doi.org/10.1080/15376494.2016.1196795.

Ebrahimi, F. and Barati, M.R. (2016b), "Dynamic modeling of a thermo–piezo-electrically actuated nanosize beam subjected to a magnetic field", *Appl. Phys. A*, **122**, 451. https://doi.org/10.1007/s00339-016-0001-3.

Ebrahimi, F. and Barati, M.R. (2017a), "Vibration analysis of piezoelectrically actuated curved nanosize FG beams via a nonlocal strain-electric field gradient theory", *Mech. Adv. Mater. Struct.*, **25**(4), 350-359. https://doi.org/10.1080/15376494.2016.1255830.

Ebrahimi, F. and Barati, M.R. (2017b), "Buckling analysis of nonlocal third-order shear deformable functionally graded piezoelectric nanobeams embedded in elastic medium", *J. Brazilian Soc. Mech. Sci. Eng.*, **39**(3), 937–952. https://doi.org/10.1007/s40430-016-0551-5.

Ebrahimi, F. and Barati, M.R. (2017c), "Through-the-length temperature distribution effects on thermal vibration analysis of nonlocal strain-gradient axially graded nanobeams subjected to nonuniform magnetic field", *J. Therm. Stresses*, **40**(5), 548-563. https://doi.org/10.1080/01495739.2016.1254076.

Ebrahimi, F., Barati, M.R. and Haghi, P. (2017d), "Thermal effects on wave propagation characteristics of rotating strain gradient temperature-dependent functionally graded nanoscale beams", *J. Therm. Stresses*, **40**(5), 535-547. https://doi.org/10.1080/01495739.2016.1230483.

Ebrahimi, F. and Barati, M.R. (2017e), "Porosity-dependent vibration analysis of piezo-magnetically actuated heterogeneous nanobeams", *Mech. Syst. Signal Pr.*, **93**, 445-459. https://doi.org/10.1016/j.ymssp.2017.02.021.

Ebrahimi, F. and Barati, M.R. (2018a), "Vibration analysis of smart piezoelectrically actuated nanobeams subjected to magneto-electrical field in thermal environment", *J. Vib. Control*, **24**(3), 549–564. https://doi.org/10.1177/1077546316646239.

Ebrahimi, F. and Barati, M.R. (2018b), "Stability analysis of porous multi-phase nanocrystalline nonlocal beams based on a general higher-order couple-stress beam model", *Struct. Eng. Mech.*, **65**(4), 465-476. https://doi.org/10.12989/sem.2018.65.4.465.

Ebrahimi, F. and Dabbagh, A. (2017), "Nonlocal strain gradient based wave dispersion behavior of smart rotating magneto-electro-elastic nanoplates", *Mater. Res. Express*, **4**(2), 025003. https://doi.org/10.1088/2053-1591/aa55b5.

Ebrahimi, F. and Salari, E. (2015a), "Size-dependent thermo-electrical buckling analysis of functionally graded piezoelectric nanobeams", *Smart Mater. Struct.*, **24**, 125007. https://doi.org/10.1088/0964-1726/24/12/125007.

Ebrahimi, F., Salari, E. and Hosseini, S.A.H. (2015b), "Thermomechanical vibration behavior of FG nanobeams subjected to linear and non-linear temperature distributions", *J. Therm. Stresses*, **38**(12), 1360-1386. https://doi.org/10.1080/01495739.2015.1073980.

Ebrahimi, F. and Salari, E. (2015c), "A semi-analytical method for vibrational and buckling analysis of functionally graded nanobeams considering the physical neutral axis position", CMES: Computer Modeling in Engineering & Sciences, **105**(2), 151-181. https://doi.org/10.3970/cmes.2015.105.151.

Ebrahimi, F., Ghasemi, F. and Salari, E. (2016), "Investigating thermal effects on vibration behavior of temperature-dependent compositionally graded Euler beams with porosities". *Meccanica*, **51**(1), 223-249. https://doi.org/10.1007/s11012-015-0208-y.

Ebrahimi, F. and Salari, E. (2016), "Effect of various thermal loadings on buckling and vibrational characteristics of nonlocal temperature-dependent functionally graded nanobeams", *Mech. Adv. Mater. Struct.*, **23**(12), 1379-1397. https://doi.org/10.1080/15376494.2015.1091524.

Ebrahimi, F. and Hosseini, S.H.S. (2016), "Thermal effects on nonlinear vibration behavior of viscoelastic nanosize plates", *J. Therm. Stresses*, 39(5), 606-625. https://doi.org/10.1080/01495739.2016.1160684.

Ebrahimi, F. and Mokhtari, M. (2015), "Transverse vibration analysis of rotating porous beam with functionally graded microstructure using the differential transform method", *J. Brazilian Soc. Mech. Sci. Eng.*, **37**(4), 1435-1444. https://doi.org/10.1007/s40430-014-0255-7.

Fox, L. and Parker, I.B. (1968), *Chebyshev Polynomials in* Numerical *Analysis*, Oxford University Press, London, UK.

Graphene-info. (2019), Graphene Oxide: Introduction and Market News; Metalgrass LTD, Herzerlia, Israel, https://www.graphene-info.com/graphene-oxide , (accessed: 01-June-2019)

Harris, B. (1986), *Engineering Composite Materials*, Institute of Metals, London, UK.

Javani, R., Bidgoli R.M. and Kolahchi R. (2019), "Buckling analysis of plates reinforced by Graphene platelet based on Halpin-Tsai and Reddy theories", *Steel Compos. Struct.*, **31**(4), 419-427. http://dx.doi.org/10.12989/scs.2019.31.4.419.

Karami, B., Shahsavari, D., Janghorban, M. and Tounsi, A. (2019), "Resonance behavior of functionally graded polymer composite nanoplates reinforced with graphene nanoplatelets", *Int. J. Mech. Sci.*, **156**, 94-105. https://doi.org/10.1016/j.ijmecsci.2019.03.036.

Ke, L.L., Yang, J., Kitipornchai, S. and Xiang, Y. (2009), "Flexural vibration and elastic buckling of a cracked timoshenko beam made of functionally graded materials", *Mech. Adv. Mater. Struct.,* **16**(6), 488-502. https://doi.org/10.1080/15376490902781175.

Ke, L.L., Yang, J. and Kitipornchai, S. (2013), "Dynamic stability of functionally graded carbon nanotube-reinforced composite beams", *Mech. Adv. Mater. Struct.*, **20**(1), 28-37. https://doi.org/10.1080/15376494.2011.581412.

Lam, D.C.C., Yang, F., Chong, A.C.M., Wang, J. and Tong, P. (2003), "Experiments and theory in strain gradient elasticity", *J. Mech. Phys. Solids.* **51**, 1477-1508. https://doi.org/10.1016/S0022-5096(03)00053-X.

Liang, K., Sun, Q. and Liu, X.R. (2018), "Investigation on imperfection sensitivity of composite cylindrical shells using the nonlinearity reduction technique and the polynomial chaos method", *Acta Astronaut*, **146**, 349-358. https://doi.org/10.1016/j.actaastro.2018.03.018.

Li, C., Thostenson, E.T. and Chou, T.W. (2008), "Sensors and actuators based on carbon nanotubes and their composites: A review", *Compos. Sci. Technol.*, **68**(6), 1227-1249. https://doi.org/10.1016/j.compscitech.2008.01.006.

Li, X., Bhushan, B., Takashima, K., Baek, C.W. and Kim, Y.K.. (2003), "Mechanical characterization of micro/nanoscale structures for MEMS/NEMS applications using nanoindentation techniques", *Ultramicroscopy*, **97**(1), 481-494. https://doi.org/10.1016/S0304-3991(03)00077-9.

Mao, J.J. and Zhang, W. (2019), "Buckling and post-buckling analyses of functionally graded graphene reinforced piezoelectric plate subjected to electric potential and axial forces", *Compos. Struct.*, **216**(5), 392-405. https://doi.org/10.1016/j.compstruct.2019.02.095.

Mahkam, M., Rafi, A.A., Faraji, L. and Zakerzadeh, E. (2015), "Preparation of poly (methacrylic acid)–graphene oxide nanocomposite as a pH-Sensitive drug carrier through in-situ copolymerization of methacrylic acid with polymerizable graphene", *Polymer-Plastics Technology and Engineering*, **54**(9), 916-922. https://doi.org/10.1080/03602559.2014.961081.

Mohammed, A. and Cagri, M. (2018), "Dynamic stability of sandwich functionally graded micro-beam based on the nonlocal strain gradient theory with thermal effect", *Compos. Struct.*, **201**, 1018-1030. https://doi.org/10.1016/j.compstruct.2018.06.035.

Mindlin, R.D. (1963), "Influence of couple-stresses on stress concentrations", *Exp. Mech.*, **3**, 1–7. https://doi.org/10.1007/BF02327219.

Park, S.K. and Gao, X.L. (2006), "Bernoulli–Euler beam model based on a modified couple stress theory", *J. Micromech. Microeng.*, **16**, 2355–2359. https://doi.org/10.1088/0960-1317/16/11/015.

Potts, R.J., Dreyer, R.D., Bielawski, W.C. and Ruoff, S.R. (2011), "Graphene-based polymer nanocomposites", *Polymer*, **52**(1), 5-25. https://doi.org/10.1016/j.polymer.2010.11.042.

Ramaratnam, A. and Jalili, N. (2006), "Reinforcement of piezoelectric polymers with carbon nanotubes: pathway to next-generation sensors", *J. Intel. Mat. Syst. Str.*, **17**(3), 199-208. https://doi.org/10.1177/1045389X06055282.

Reddy, J.N. (2003), *Mechanics of Laminated Composite Plates and Shells: Theory and Application*, (2nd Edition), CRC Press, New York, Washington D.C., USA.

Rokni, H., Milani, A.S. and Seethaler, R.J. (2012a), "Improvement in dynamic properties of laminated MWCNT-polystyrene composite beams via an integrated numerical–experimental approach", *Compos. Struct.*, **94**(8), 2538-2547. https://doi.org/10.1016/j.compstruct.2012.03.028.

Rokni, H., Milani, A.S. and Seethaler, R.J. (2012b), "2D optimum distribution of carbon nanotubes to maximize fundamental natural frequency of polymer composite micro-beams", *Compos. Part B: Eng.*, **43**(2), 779-785. https://doi.org/10.1016/j.compositesb.2011.07.012.

Saemul, S. and Ganesan, R. (2018), "Dynamic instability of rotating doubly-tapered laminated composite beams under periodic rotational speeds", *Compos. Struct.*, **200**, 711-728. https://doi.org/10.1016/j.compstruct.2018.05.133.

Setoodeh, A. and Rezae, M. (2017), "Large amplitude free vibration analysis of functionally graded nano/micro beams on nonlinear elastic foundation", *Struct. Eng. Mech.*, **61**(2), 209-220. http://dx.doi.org/10.12989/sem.2017.61.2.209.

Shi, G. (2007), "A new simple third-order shear deformation theory of plates", *Int. J. Solids Struct*., **44**(13), 4399-4417. https://doi.org/10.1016/j.ijsolstr.2006.11.031.

Song, M., Kitipornchai, S. and Yang, J. (2016), "Free and forced vibrations of functionally graded polymer composite plates reinforced with graphene nanoplatelets", *Compos. Struct.*, **159**, 579-588. https://doi.org/10.1016/j.compstruct.2016.09.070.

Trinh, C.L., Vo, P.T., Thai, H.T. and Nguyen, T.K. (2018), "Size-dependent vibration of bi-directional functionally graded microbeams with arbitrary boundary conditions", *Compos. Part B: Eng.*, **134**, 225-245. https://doi.org/10.1016/j.compositesb.2017.09.054.

Van Es, M.A. (2001), "Polymer-clay nanocomposites: the importance of particle dimensions", Ph.D. Dissertation, Delft University of Technology, Delft, Netherlands.

Wang, A., Chen, H., Hao, Y. and Zhang, W. (2016), "Vibration and bending behavior of functionally graded nanocomposite doubly-curved shallow shells reinforced by graphene nanoplatelets", *Results in Physics*, **9**, 550-559. https://doi.org/10.1016/j.rinp.2018.02.062.

Wang, Y., Xie, K., Fu, T. and Shi, C. (2019a), "Vibration response of a functionally graded graphene nanoplatelet reinforced composite beam under two successive moving masses", *Compos. Struct.*, **209**, 928-939. https://doi.org/10.1016/j.compstruct.2018.11.014.

Wang, Y., Xie, K., Shi, C. and Fu, T. (2019b), "Nonlinear bending of axially functionally graded microbeams reinforced by graphene nanoplatelets in thermal environments", *Mater. Res. Express*, **6**, 085615. https://doi.org/10.1088/2053-1591/ab1eef.

Wattanasakulpong, N., Gangadhara, B.P. and Donald, W.K. (2011), "Thermal buckling and elastic vibration of third-order shear deformable functionally graded beams", *Int. J. Mech. Sci.*, **53**(9), 734-743. https://doi.org/10.1016/j.ijmecsci.2011.06.005.

Wattanasakulpong, N. and Bui, T.Q. (2018), "Vibration analysis of third-order shear deformable FGM beams with elastic support by Chebyshev collocation method", *Int. J. Struct. Stability Dynam.*, **18**(5), 1850071. https://doi.org/10.1142/S0219455418500712.

Weon, J.I. (2009), "Mechanical and thermal behavior of polyamide-6/clay nanocomposite using continuum-based micromechanical modeling", *Macromol. Res.*, **17**(10), 797-806. https://doi.org/10.1007/BF03218617.

Wu, H., Yang, J. and Kitipornchai, S. (2017), "Dynamic instability of functionally graded multilayer graphene nanocomposite beams in thermal environment", *Compos. Structu.*, **162**(15), 244-254. https://doi.org/10.1016/j.compstruct.2016.12.001.

Xin, J. Wang, J. and Yao, J. (2011), "Vibration, buckling and dynamic stability of a cracked cylindrical shell with time-varying rotating speed", *Mech. Based. Des. Struct. Mach. Int. J.*, **39**(4), 461-490. https://doi.org/10.1080/15397734.2011.569301.

Yang, F., Chong, A.C.M., Lam, D.C.C. and Tong, P. (2002), "Couple stress based strain gradient theory for elasticity", *Int. J. Solids Struct.*, **39**(10), 2731-2743. https://doi.org/10.1016/S0020-7683(02)00152-X.

Yang, S.Y., Lin, W.N., Huang, Y.L., Tien, H.W., Wang, J.Y., Ma, M.C.C, Li, S.M. and Wang Y.S. (2010), "Synergetic effects of graphene platelets and carbon nanotubes on the mechanical and thermal properties of epoxy composites", *Carbon*, **49**(3), 793-803. https://doi.org/10.1016/j.carbon.2010.10.014.

Zhang, Z., *et al*. (2018), "Mechanical analysis of functionally graded graphene oxide-reinforced composite beams based on the first-order shear deformation theory", *Mech. Adv. Mater. Struct.*, (In press). https://doi.org/10.1080/15376494.2018.1444216.

Zhou, D., Lo, S.H., Au, F.T.K., Cheung, Y.K. and Liu, W.Q. (2006), "3-D vibration analysis of skew thick plates using Chebyshev–Ritz method", *Int. J. Mech. Sci.*, **48**(12), 1481-1493. https://doi.org/10.1016/j.ijmecsci.2006.06.015.

CC